COMMUNICATIONS IN SCIENCE AND TECHNOLOGY
Homepage: cst.kipmi.or.id

Physicochemical and antibacterial properties of green-synthesized bimetallic CuO-ZnO nanoparticles

Ni Ketut Eri Suryani, I Wayan Karyasa*, I Putu Parwata

Department of Chemistry; Universitas Pendidikan Ganesha, Singaraja 81117, Indonesia

Article history:
Received: 2 May 2026 / Received in revised form: 19 June 2026 / Accepted: 19 June 2026

Abstract

Green-synthesized bimetallic copper oxide–zinc oxide (CuO/ZnO) nanoparticles have attracted considerable interest due to their enhanced physicochemical properties and antibacterial activity. This study proposes a green synthesis approach for CuO/ZnO nanoparticles and evaluates their physicochemical characteristics and antibacterial performance by means of a range of analytical techniques including XRD, XRF, FTIR, SEM–EDX, and UV–Visible spectroscopy. XRD analysis confirmed elevated crystallinity in all samples, while the CuO/ZnO bimetallic variant (Cbest) exhibited the smallest crystallite size (22.93 nm). Antibacterial assays, conducted utilizing the agar well diffusion method demonstrated that pure CuO nanoparticles exhibited the strongest inhibition against *Escherichia coli* (15.39 mm), whereas the CuO/ZnO bimetallic variant (Cbest) demonstrated the highest activity against *Staphylococcus aureus* (10.02 mm). The results of the one-way ANOVA indicated significant differences among the treatments ($p < 0.05$), thus confirming the influence of nanoparticle composition on antibacterial efficacy. These findings highlight the potential of green-synthesized CuO/ZnO nanoparticles as effective antibacterial agents.

Keywords: Copper-zinc; antibacterial activities; moringa oleifera

1. Introduction

Antibiotic-resistant microorganisms have been observed to be increasing worldwide, necessitating an urgent development of alternative antimicrobial agents. Metal oxide nanoparticles, including Copper Oxide (CuO) and Zinc Oxide (ZnO), have emerged a promising alternatives due to their intrinsic biocidal properties, robust chemical stability, and cost-effectiveness. The antibacterial activity of biosynthesized ZnO nanoparticles has been demonstrated against both *Staphylococcus aureus* (Gram-positive) and *Escherichia coli* (Gram-negative), in addition to exhibiting excellent photocatalytic degradation capabilities [1]. Furthermore, previous studies have demonstrated that chitosan–ZnO nanoparticles effectively inhibited the proliferation of *Escherichia coli*, with the antibacterial efficacy increasing in a concentration-dependent manner, as evidenced by the enlargement of the inhibition zone [2]. Similarly, copper nanoparticles have been demonstrated to possess strong antibacterial properties, effectively suppressing the growth of four different microbial strains [3]. Consequently, the integration of copper and zinc into a bimetallic nanoparticle system is anticipated to generate synergistic effects, leading to enhanced antibacterial efficacy relative to the individual monometallic nanoparticles.

The utilization of green synthesis methodologies is increasingly favored over the conventional chemical routes in view of environmental concerns. These processes utilize biological extracts as sustainable bio-reductants and capping agents. These extracts provide a complex matrix of phytochemicals including flavonoids, phenols, and terpenes [4]. These biomolecules contribute significantly to the nucleation, stabilization, and biocompatibility of the formed nanoparticles.

In the domain of green synthesis of nanoparticles, *Moringa oleifera* leaf extract has emerged as a promising candidate among the various plant extracts utilized as bio-reducing agents. This is due to its rich phytochemical composition. Moringa leaves have been shown to contain various secondary metabolites, including flavonoids, alkaloids, tannins, saponins, and terpenoids [5]. The utilization of moringa leaves in the synthesis of Ag nanoparticles has also been demonstrated to

* Corresponding author. Tel.: +62-813-5394-4585
Email: karyasa@undiksha.ac.id
https://doi.org/10.21924/cst.11.1.2026.1976

facilitate the reduction of Ag^+ to Ag^0 at the nanoscale in addition to inhibiting the growth of *Escherichia coli*, thereby producing inhibition zones of 1.44 cm and 1.25 cm [6]. This finding provides evidence that *Moringa oleifera* leaf extract can be utilized as a bio-reducing agent in nanoparticle synthesis and demonstrates its potential for antibacterial applications in view of the combined antibacterial effects of the leaf extract and the metal oxides involved in nanoparticle formation.

Despite the significant advances achieved in the development of bimetallic nanoparticles, there are several critical gaps that still need to be addressed. A comprehensive understanding of the way synthesis parameters, including pH, temperature, and calcination conditions, to influence the resulting physicochemical properties of bimetallic systems remains underexplored. Most reported studies are case-specific and fail to establish the design principles with broad applicability. In addition, the mechanistic role of individual phytochemical constituents in regulating nucleation kinetics and promoting p–n heterojunction formation has not yet been fully elucidated.

The current understanding of the synergistic antibacterial mechanisms of bimetallic CuO/ZnO nanoparticles remains incomplete. Despite the recognized antibacterial effects of these systems, which are associated with the generation of reactive oxygen species (ROS), membrane disruption, and metal ion release, the relative contribution of each mechanism under different environmental conditions, such as light and dark settings, has not been fully elucidated. Furthermore, the role of CuO/ZnO heterojunctions in facilitating charge transfer and suppressing charge carrier recombination, which are critical processes for enhanced ROS generation, remains poorly understood. Therefore, further fundamental studies are necessitated to clarify the mechanistic relationship between heterojunction formation and antibacterial performance.

It is evident that the natural variation of biological precursors frequently leads to instability in the process of green synthesis. Batch-to-batch variability in morphology and composition represents a bottleneck for industrial translation. At present, the field is characterized by the devoid of standardized quality control protocols, techno-economic analyses, and comprehensive Life Cycle Assessments (LCA). This paucity of data raises questions regarding the feasibility and sustainability of large-scale production, especially in regulated fields such as wastewater treatment and biomedical engineering. Moreover, there is a conspicuous absence of long-term toxicological studies. While green synthesis is expected to enhance biocompatibility, data related to the chronic accumulation of nanoparticles in biological systems and the potential ecotoxicological risks of dissolved Cu^{2+} and Zn^{2+} ions to aquatic and terrestrial organisms are inadequate.

The research advancement provides a multiscale framework that integrates green chemistry with advanced characterization and sustainability metrics. This approach entails the optimization of ROS-mediated activity with a focus on the structure–property–function relationship, particularly through the utilization of heterojunction engineering. The ultimate objective is to transition towards a paradigm of "bio-directed nanostructure engineering," wherein the chemical diversity inherent in biological extracts is regarded not as an uncontrolled variable, but rather as a tunable parameter. This paradigm shift is expected to facilitate the translation of innovations at the laboratory scale to the real-world application of next-generation antimicrobial nanomaterials.

2. Materials and Methods

2.1. Materials

The experimental research study employed moringa leaves (*Moringa oleifera*) waste collected from Herbal Nusantara; in addition to copper acetate monohydrate ($Cu(CH_3COO)_2 \cdot H_2O$), ACS Reagent, 99%; Zinc chloride hexahydrate ($ZnCl_2 \cdot 6H_2O$), ACS Reagent, 98%; Sodium hydroxide, ACS Reagent, 97% (NaOH); and Ethanol 98% (OneMed).

2.2. Preparation of Moringa oleifera leaves extract

Moringa oleifera leaf was collected from Herbal Nusantara. The object was subsequently subjected to a process of cleaning and sun-drying for a period of 72 hours. The extraction process was conducted by macerating 500 g of leaf powder in 5000 mL of 96% ethanol at a 1:10 (w/v) ratio also for a period of 72 hours [6]. The resulting mixture was then subjected to vacuum filtration to separate the extract from the plant residue.

2.3. Synthesis of CuO nanoparticles

The synthesis of copper oxide (CuO) nanoparticles was performed through the dissolution of 19.965 g of copper (II) acetate monohydrate in 100 mL of distilled water. Subsequently, 200 mL of *Moringa oleifera* leaf extract was added to the solution. The addition of NaOH was conducted dropwise, with the objective of reducing the pH level of the mixture to 8. Following this, the mixture was heated to 80°C and stirred using a magnetic stirrer for 1.5 hours until the change of color to brownish and the formation of a precipitate was observed. Upon the completion of the reaction, the solution was subjected to a centrifugal process at a speed of 3000 RPM for a duration of 20 minutes purposely to separate the supernatant from the precipitate. The obtained precipitate was then dried in an oven at a temperature of 80°C for a period of approximately 3 hours. Finally, the dried nanoparticles were calcined in a furnace at 500°C within 2 hours to form the oxide of Cu.

2.4. Synthesis of ZnO nanoparticles

The synthesis of zinc oxide (ZnO) nanoparticles was performed by means of the dissolution of 13.629 g of zinc

chloride hexahydrate in 100 mL of distilled water. Subsequently, 200 mL of *Moringa oleifera* leaf extract was added to the solution. The pH of the mixture was then adjusted to 8 by the dropwise addition of NaOH. The resulting solution was subjected to heating at 80°C and stirred using a magnetic stirrer for a duration of 1 hour and 30 minutes until the change of color to yellowish-green and the formation of a precipitate were identified. Having observed the reaction, the mixture was centrifuged at 3000 RPM for a duration of 20 minutes to separate the precipitate from the supernatant. The obtained precipitate was dried in an oven at a temperature of 80°C for a period of approximately 3 hours. Finally, the dried nanoparticles were calcined in a furnace at 500°C for 2 hours to form the oxide of Zn.

2.5. Synthesis of CuO-ZnO nanoparticles

The synthesis of nanoparticles commenced with the preparation of a beaker containing 100 mL each of copper (II) acetate monohydrate and zinc chloride hexahydrate solutions. Subsequently, 200 mL of *Moringa oleifera* leaf extract was added to the solution. The pH of the mixture was then adjusted to 8 by the dropwise addition of NaOH. The resulting solution was subjected to heating at a temperature of 80°C, followed by stirring using a magnetic stirrer for a duration of 1 hour and 30 minutes. This process resulted in the observation of a yellowish-green color change and the formation of a precipitate. Following this, the mixture was centrifuged at 3000 RPM for a duration of 20 minutes with the objective of isolating the precipitate from the supernatant. The precipitate obtained was then dried in an oven at a temperature of 80°C for 1 hour. Finally, the dried nanoparticles were calcined in a furnace at a temperature of 500°C for 2 hours to form the oxide, and the mass of the oxide was determined by weighing to the yield.

2.6. Characterization of nanoparticles

Scanning electron microscopy (SEM, Hitachi FlexSEM-1000) with an accelerating voltage of 20 kV and a magnification of 30.000x was utilized to analyze the morphology, elemental composition, and elemental mapping of the samples. The identification of the functional groups included in the nanocomposites was facilitated by means of Fourier-Transform Infrared (FTIR, Shimadzu IRTracer-100) spectroscopy within the wavenumber range of 4000–400 cm^{-1}. The crystal structure was characterized by X-ray Diffraction (XRD, Rigaku Miniflex 300/600) over a 2θ range of 0°–90° with an X-ray source of Cu Kα1 ($\lambda = 0.154$ nm). UV-Vis spectroscopy (UV-2600i Plus) was employed to determine the band gap energy within the wavelength range of 200–400 nm. Furthermore, X-ray fluorescence (XRF) was utilized to quantify the chemical composition and determine the particle size distribution, respectively. The mean crystal size can be determined through the Debye-Scherrer equation.

$$D = \frac{K\lambda}{\beta cos\theta} \quad (1)$$

where:
D = average crystallite size (nm)
K = Scherrer constant or shape factor (0.94)
λ = wavelength of the X-ray radiation utilized (nm)
β = full width at half maximum (FWHM) of the diffraction peak (radians)
θ = Bragg diffraction angle (half of the measured 2θ value)

2.7 Antibacterial activity

The evaluation of the antibacterial activity against Gram-positive (*Staphylococcus aureus*) and Gram-negative (*Escherichia coli*) bacteria was conducted through agar well diffusion method. The diameter of the inhibition zone was measured in triplicate by means of a digital caliper in four different directions. A one-way analysis of variance (ANOVA) was employed to ascertain any significant differences among treatment groups, with a significance level of $p < 0.05$. The net inhibition zone diameter was calculated by subtracting the diameter of the well from the average diameter of the clear zone according to Equation (1):

$$\boldsymbol{T = \frac{D1+D2+D3+D4}{4} - X} \quad (2)$$

where *T* represents the net inhibition zone diameter (mm), *D1, D2, D3,* and *D4* refer to the inhibition zone diameters measured in four different directions (mm), and *X* is the diameter of the agar well (mm).

3. Results and Discussion

3.1. Nanoparticle characterization

3.1.1. UV-Visible analysis

The UV-Vis spectra provide significant evidence for the formation of metal oxide nanoparticles through the green synthesis route, as illustrated in Fig. 1. The absorption peak observed in the system that contained the extract was found to be associated with the presence of phenolic and flavonoid compounds, which are identified to function as reducing, chelating, and stabilizing agents during the synthesis of nanoparticle. The addition of $Cu(CH_3COO)_2$ was observed to result in a decrease in the intensity of absorbance, indicating the involvement of hydroxyl groups in the reduction and complexation of Cu^{2+} ions. In the presence of an alkaline conditions, phenolic compounds such as quercetin undergo a process of deprotonation, resulting in the formation of phenolate ions, which exhibit a capacity for coordination with metal ions leading to subsequent oxidation and the formation of quinone derivatives. This oxidation process has been shown to release electrons, thereby facilitating the conversion of metal ions into metal oxide nanoparticles [7,8].

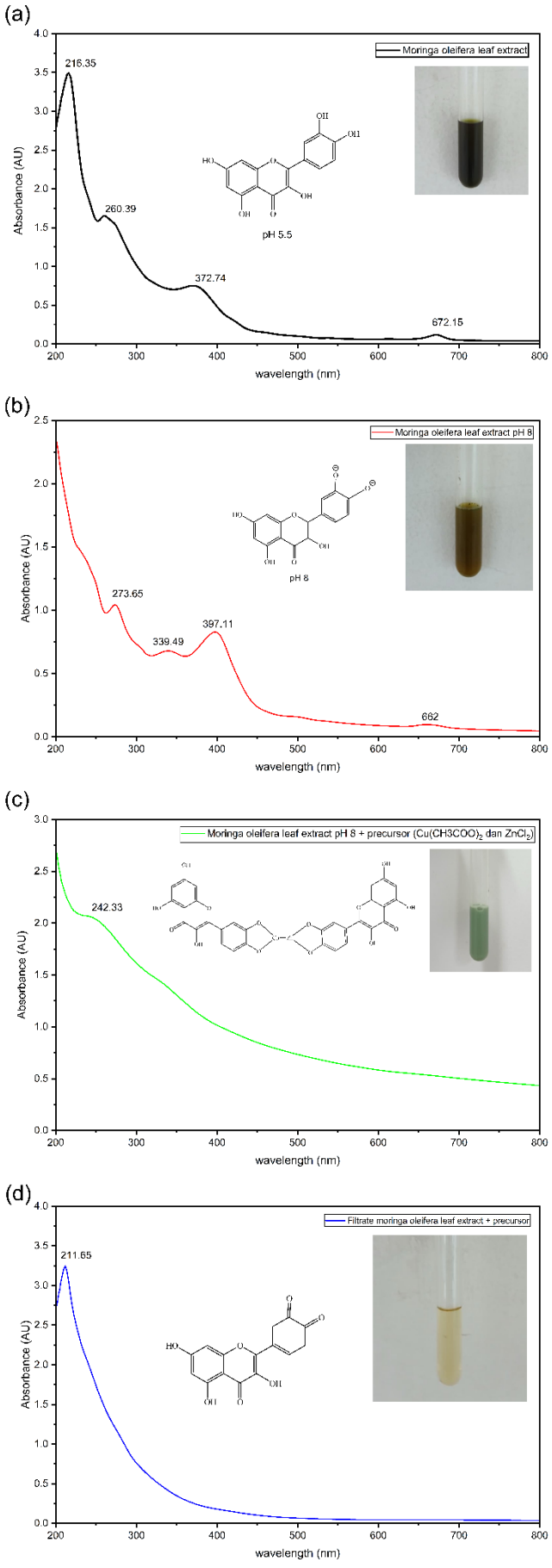

Fig. 1. UV-Vis Spectra: (a) CuO-NPs; (b) ZnO-NPs; (c) CuO/ZnO NPs

The absorption band that has been observed for CuO nanoparticles in the 260–300 nm region is attributed to charge-transfer transitions and is commonly associated with nanosized CuO structures [9]. The reduction in the intensity of absorbance following the addition of precursor provides further evidence for the consumption of phytochemicals during the process of nanoparticle formation. In green synthesis systems, Cu^{2+} ions initially form complexes with phenolic compounds prior to undergoing hydrolysis and dehydration reactions that eventually yield CuO nanoparticles [10].

Conversely, ZnO nanoparticles exhibited an absorption band at approximately 360–370 nm, which is in alignment with the intrinsic band-gap absorption characteristics of ZnO nanoparticles. This absorption feature is widely recognized as evidence of ZnO formation and reflects electronic excitation from the valence band to the conduction band [11,12]. The formation of ZnO is commonly theorized to occur via the conversion of Zn^{2+} ions into $Zn(OH)_2$ in the presence of alkaline conditions, precipitated by thermal or spontaneous dehydration to ZnO nanoparticles [13].

The UV–Vis spectrum of the bimetallic CuO/ZnO nanocomposite exhibited a broader absorption profile extending from 300 to 450 nm in comparison to those of the monometallic CuO and ZnO systems. Such broadening is indicative of the occurrence of electronic interactions between the two metal oxides, which suggests the successful formation of a heterojunction within the nanocomposite structure. The combination of CuO and ZnO has been shown to modify the electronic environment, thereby promoting charge redistribution at the interface. This, in turn, results in altered optical properties and enhanced absorption over a wider wavelength range [14,15]. Consequently, the observed spectral changes provide substantial evidence that the phytochemicals present in the extract not only facilitate the conversion of Cu^{2+} and Zn^{2+} ions into their corresponding oxides but also induce the formation of a CuO/ZnO nanocomposite through simultaneous nucleation, growth, and stabilization processes.

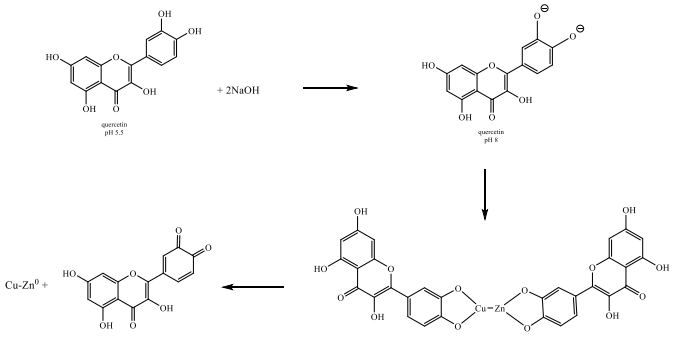

Fig. 2. Reaction mechanism of nanoparticle formation

The formation of CuO/ZnO nanoparticles is hypothesized to occur through a series of reduction, complexation, hydrolysis, and nucleation processes mediated by phytochemicals present in *the Moringa oleifera* leaf extract (see Fig. 2). Phenolic and flavonoid compounds, particularly

quercetin-like molecules, have been observed to contain hydroxyl groups that possesses the capacity to coordinate with Cu^{2+} and Zn^{2+} ions. In the presence of an alkaline environment, these hydroxyl groups undergo a process of deprotonation to form phenolate ions, which readily bind metal ions and facilitate the formation of metal–organic complexes. Simultaneously, the phenolic compounds undergo oxidation to quinone derivatives, resulting in the release of electrons that facilitate the transformation of metal precursors into metal oxide nuclei. Subsequently, Cu^{2+} and Zn^{2+} ions undergo hydrolysis to form $Cu(OH)_2$ and $Zn(OH)_2$ intermediates, which are further converted into CuO and ZnO nanoparticles through dehydration reactions. The continuous growth and aggregation of these nuclei ultimately result in the formation of a CuO/ZnO nanocomposite, while the phytochemicals adsorbed on the nanoparticle surface act as capping and stabilizing agents, thereby preventing excessive particle agglomeration [7,8,10].

3.1.2. Fourier transform infrared spectroscopy (FTIR) analysis

FTIR spectra were employed to inspect the characteristic impurities and functional groups present within the particles. The FTIR spectra as depicted in Fig. 3 illustrate a comparison between ZnO-NPs, CuO-NPs, and CuO/ZnO nanocomposites at different ratios throughout the wavenumber range 4000-400 cm^{-1}. In the spectrum of ZnO-NPs, a sharp absorption peak is observed at 534 cm^{-1}, which corresponds to the stretching vibration of the Zn–O bond. This finding is consistent with the extant literature, which asserts that Zn–O vibrations typically emerge within the 400–600 cm^{-1} range. Furthermore, the CuO spectrum exhibits a peak at 558 cm^{-1}, confirming the Cu–O bond vibration, and indicating the formation of the monoclinic phase of copper oxide. In the CuO/ZnO spectra (for both the optimum condition and the 1:1 ratio), wavenumber shifts to 539 cm^{-1} and 558 cm^{-1} were observed.

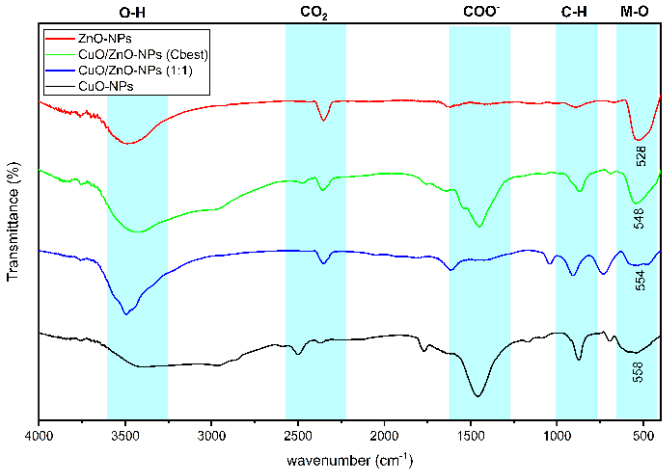

Fig. 3. Comparison of FTIR Spectra CuO-NPs, ZnO-NPs, and CuO/ZnO NPs

The presence of these peaks demonstrates the successful formation of the nanocomposite structure, while the inherent characteristics of both constituent metal oxides are maintained. Additionally, the broad absorption observed in the range of 3462–3490 cm^{-1} is indicative of the stretching vibration of –OH groups present in polyphenolic compounds, such as quercetin. These compounds are abundant in *Moringa oleifera*. The strong intensity observed in the CuO/ZnO samples correlates with enhanced particle stability, which in turn effectively prevents agglomeration.

3.1.3. X-ray diffraction (XRD) analysis

X-ray diffraction (XRD) analysis has been used to confirm the formation of monoclinic CuO and hexagonal wurtzite ZnO phases in bimetallic systems. The size of nanoparticle typically ranges from 5 to 50 nm dependent upon the synthesis conditions [2].

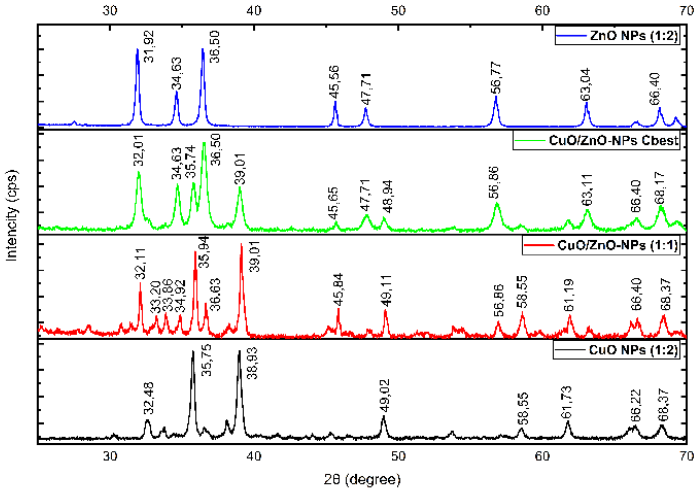

Fig. 4. XRD pattern of CuO-NPs, ZnO-NPs, and CuO/ZnO NPs

Fig. 4 illustrates the XRD patterns of the synthesized CuO, ZnO, and CuO/ZnO nanoparticles. The XRD pattern of CuO nanoparticles exhibits diffraction peaks at 2θ:, The following values are indexed to the reflection planes of (110), (-111), (111), (-202), (202), and (-113), respectively: 32,48°, 35.75°, 38.93°, 49.02°, 58.55°, 61.73°, 66.22°, and 68.37°. The crystal planes thus provide strong confirmation of the monoclinic structure of the CuO nanoparticles, as further validated by comparison with the COD database No. 1011194 [16]. For the ZnO nanoparticles, peaks are observed at 2θ: with the following observed values of 31.92°, 34.63°, 36.50°, 47.71°, 56.77°, 63.04°, 66.40°, and 68.09°, corresponding to the (100), (002), (101), (102), (110), (103), (200), and (112) planes. The planes confirm the hexagonal wurtzite structure of ZnO, which is consistent with COD No. 2107059 [17]. In the CuO/ZnO-NPs (1:1) sample, the (111) peak exhibits the highest intensity, indicating that most of the crystals are dominated by the (111) plane. Furthermore, as demonstrated in Fig. 4, the intensities of the peaks associated with CuO in the CuO/ZnO diffraction pattern appear higher than those of the ZnO peaks. This finding indicates a higher crystalline percentage of CuO within the bimetallic structure and indicates high overall crystallinity.

In the XRD pattern of the CuO/ZnO-NPs (Cbest), as illustrated in Fig. 4, the (101) plane exhibits the highest intensity, thereby indicating that the crystal structure is predominantly oriented along this plane. Furthermore, as depicted in Fig. 4, the peak intensities associated with ZnO in the CuO/ZnO diffraction pattern appear higher than those of the CuO nanoparticles. The lower crystallinity and peak intensity of CuO-NPs within the composite have been linked to the coating effect of ZnO-NPs on the CuO-NPs, which then protects the copper layer from further oxidation. In both composite materials, no significant peak shifts were observed, suggesting that both phases maintain their respective crystalline integrity without the formation of a new solid solution. This phenomenon states that in CuO/ZnO heterostructure systems, both materials tend to grow separately while forming a robust interfacial contact.

Table 1. Crystal size of CuO-NPs, ZnO-NPs, and CuO/ZnO-NPs

Materials	Crystal size (nm)	Standard Deviation (SD)
CuO	39.01	24.53
ZnO	48.24	12.70
CuO/ZnO (1:1)	40.90	18.87
CuO/ZnO (Cbest)	22.94	11.83

The results of the Debye-Scherrer equation results (see Table 1) demonstrate that the average crystallite size of the monometallic CuO nanoparticles was 39.01 nm, while ZnO exhibited a larger size of 48.24 nm. This variation in crystallite size is associated with the distinct nucleation and crystal growth rates of each metal during the green synthesis process. Secondary metabolites (for instance, flavonoids and polyphenols) function as growth-limiting factors in green synthesis systems mediated by plant extracts. The larger crystallite size of ZnO suggests that the growth of the wurtzite phase tends to be more dominant under the equivalent calcination temperatures in comparison to the monoclinic structure of CuO.

An interesting phenomenon was observed in the bimetallic samples. The CuO/ZnO (1:1) sample exhibited a crystallite size of 40.90 nm, which falls between the sizes of its two monometallic constituents. However, in the CuO/ZnO (Cbest) sample, a significant reduction in crystallite size to 22.94 nm was observed. This decrease in crystallite size within the 'Cbest' bimetallic system indicates the occurrence of cross-growth inhibition. The presence of Cu atoms within the Zn lattice or surface (and vice versa) has been demonstrated to disrupt orderly crystal growth, thereby triggering more extensive nucleation and resulting in smaller crystalline dimensions.

The crystallite size and crystallinity of the synthesized nanoparticles are found to be significantly influenced by the phytochemicals present in the *Moringa oleifera* leaf extract. Phenolic compounds, flavonoids, tannins, and other bioactive constituents function not only as reducing agents but also as capping and stabilizing agents during the process of nanoparticle formation. These compounds adsorb onto the surface of growing nuclei, thereby limiting crystal growth and preventing excessive particle agglomeration. Consequently, a larger number of nucleation sites are generated, resulting in the formation of nanoparticles with reduced crystallite sizes. Analogous observations have been reported in green synthesis systems, where plant-derived phytochemicals regulate the nucleation and growth kinetics of metal oxide nanoparticles [7,8].

Furthermore, the interaction between phytochemicals and metal ions has the capacity to affect the crystallization process, consequently determining the degree of crystallinity. The process of adsorption of organic molecules on specific crystal facets has been shown to hinder preferential crystal growth, thus resulting in changes in crystallite size and crystallinity. A higher concentration of phytochemicals has been demonstrated to commonly promote nucleation over crystal growth, producing smaller crystallites with broader diffraction peaks. Conversely, lower concentrations may favor crystal growth and higher crystallinity.

3.1.4. Scanning electron microscopic-energy dispersive X-ray (SEM-EDX)

Scanning electron microscopy (SEM) analysis reveals diverse morphologies including spherical, rod-like, and flower-like nanostructures. As illustrated in Fig. 5, significant morphological differences resulting from the different types of metal precursors used are observed. The CuO nanoparticles (see Fig. 5(a) exhibit a particle morphology that tends to be spherical and granular. Agglomeration was observed forming large clusters with submicron sizes, consistent with the particle size distribution histogram ranging from 18–32 nm as depicted in Fig. 6(a). This is a common characteristic of metal oxide nanoparticles, which exhibit high surface energy [18]. ZnO nanoparticles (Fig. 5(b)) demonstrate a significantly smaller particle morphology, with a range of 12–35 nm (Fig. 5b) that are more dispersed than CuO. The morphology of the samples examined is consistent with a hypothesis of densely packed fine grains, indicating a higher specific surface area.

As illustrated in Fig. 5(c), a pronounced morphological transformation occurs, resulting in the formation of irregular layered nanosheets or flower-like structures. These structures exhibit a particle size distribution ranging from 22–36 nm (see Fig. 6(c)). The presence of two distinct metal phases (Cu and Zn) within a single system leads to crystal growth modification, where the interaction between Cu and Zn atoms inhibits isotropic growth, resulting in the formation of unique planar structures. In contrast to the nanosheet structures observed in other ratios, Fig. 5(d) displays an assembly of nanometer-sized primary particles forming a sponge-like structure with a particle size distribution ranging from 15–26 nm (Fig. 6(d)). This structure is highly advantageous for functional applications as it provides a substantial active surface area. The observed agglomeration phenomenon is likely attributable to

strong inter-surface interactions during the drying or calcination processes.

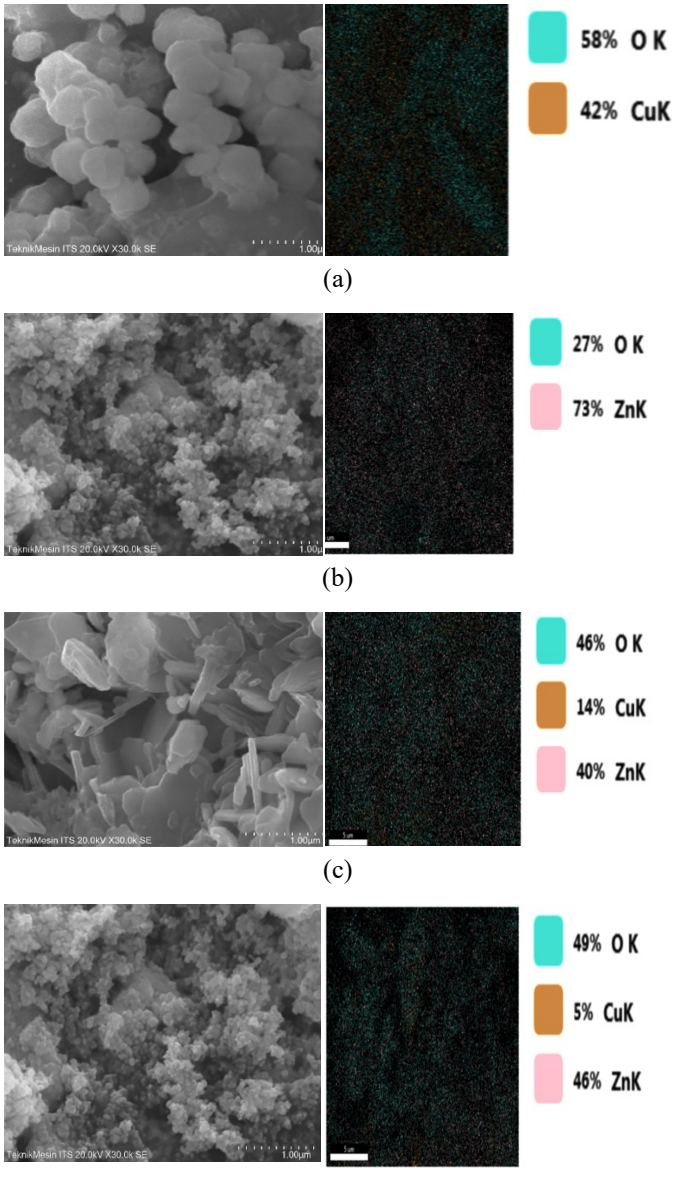

Fig. 5. SEM images of: (a) CuO-NPS; (b) ZnO-NPs; (c) CuO/ZnO-NPs 1:1; (d) CuO/ZnO-NPs CBest

3.1.4. X-Ray Fluorescence (XRF) analysis

X-ray fluorescence (XRF) was utilized to determine the elemental composition and purity of the nanoparticles synthesized employing the green synthesis approach. The results of XRF analysis are presented in Fig. 7.

As illustrated in Fig. 7(a), the elemental distribution is found to be relatively complex. Despite the objective of green synthesis approach of producing high-purity nanoparticles, the presence of accompanying elements is prevalent due to the utilization of natural precursors (plant extracts). The dominance of the CuO component at 78.2% (Fig. 7(a)) indicates the successful formation of metal-based materials. Green synthesis frequently yields nanoparticles with purity levels ranging between 70% and 90%, with the remaining proportion consisting of leftover biomolecules from the plant extract that serve as capping agents [19]. The high copper concentration (in oxide form) is a key parameter for the successful reduction of Cu^{2+} ions into CuO nanoparticles, mediated by reducing agents derived from the plant extract, such as flavonoids or polyphenols. Furthermore, the presence of MgO (15.35%) and Al_2O_3 (5.17%) is of considerable significance. This phenomenon is likely attributable to the source plants, which absorb minerals (magnesium and aluminum) from the soil, subsequently accumulating in the extract and precipitating during the calcination process.

The successful formation of zinc oxide (ZnO) nanoparticles with a mass percentage of 74.71% is depicted in Fig. 7(b). This high ZnO content demonstrates that the *Moringa oleifera* leaf extract effectively acted as both a reducing and stabilizing agent (capping agent), converting the zinc salt precursor into its oxide form. A significant finding in this data is the presence of chlorine (Cl) at 20.35%. The elevated Cl content is presumably attributable to the utilization of the zinc chloride ($ZnCl_2$) precursor, indicating that the chloride ions were either not eliminated during the washing process or were entrapped within the pores of the nanoparticles encapsulated by the organic compounds of the extract. The purity of green-synthesized ZnO nanoparticles is found to be highly dependent on the intensity of the washing process and the calcination temperature [20].

The XRF analysis results presented in Fig. 7(c) reveal the presence of ZnO at 40.05%, with the other primary component identified as CuO at 42.2%. In the bimetallic research design with a 1:1 precursor ratio, the dominance of these two phases (totaling ~82.25%) confirms the success of the co-precipitation or simultaneous bio-reduction of Cu^{2+} and Zn^{2+} ions. The percentage ratio, which closely approaches an equal value (1:1), suggests that the encapsulation efficiency by the extract's biomolecules towards both metals occurred competitively and in a balanced manner. Furthermore, the detection of chlorine (Cl) at 12.58% in the sample indicates a reduction in comparison to its monometallic ZnO counterpart. Residual chloride precursors are frequently entrapped within the organic capping agent matrix of plant extracts, necessitating calcination stages or repeated washing with distilled water to minimize such impurities [21].

In contrast to the CuO/ZnO (1:1) nanoparticles, the CuO/ZnO (Cbest) nanoparticles exhibited a ZnO content of 51.44% and a CuO content of 24.3%, indicating that the zinc oxide phase is more dominant than the copper oxide phase in the resulting nanoparticle structure. The total target oxide phases reaching ~75.74% are indicative of high bio-reduction efficiency, which is mediated by the secondary metabolites of the plant extract. The presence of the Al_2O_3 component in all four nanoparticles is indicative of the intrinsic characteristics of the green synthesis process, originating from the plant extract's secondary metabolites that serve as stabilizing agents to prevent nanoparticle agglomeration.

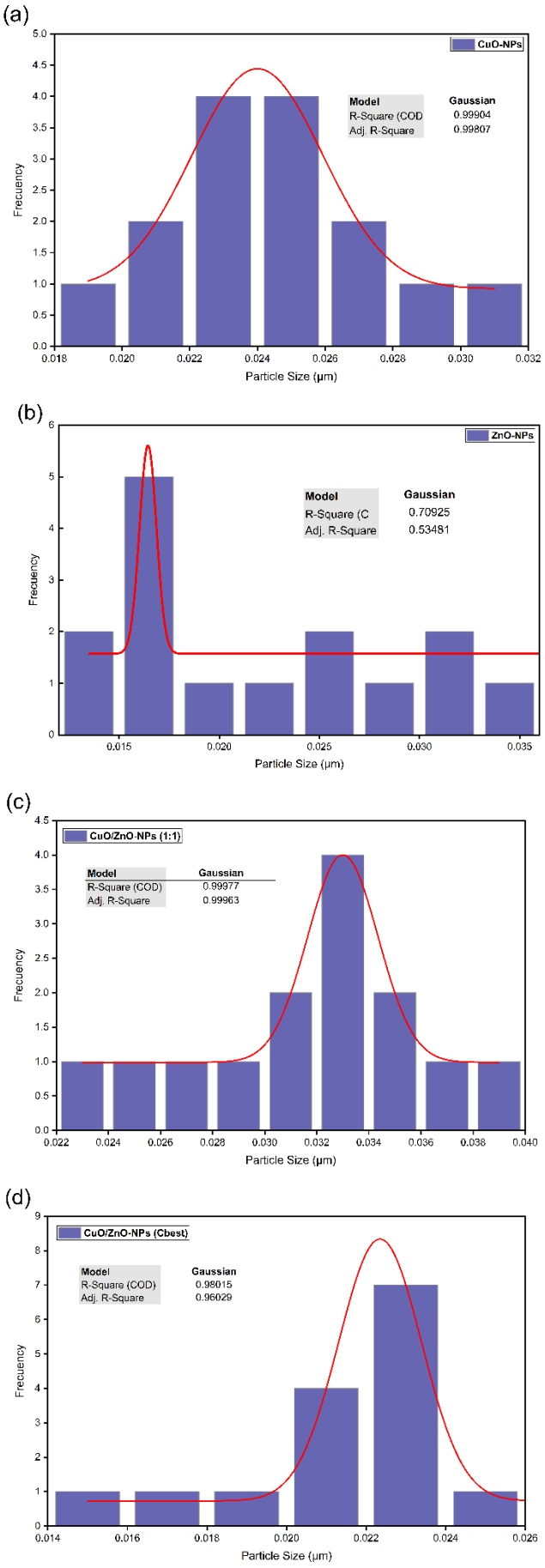

Fig. 6. Particle distribution of: (a) CuO-NPs; (b) ZnO-NPs; (c) CuO/ZnO-NPs 1:1; (d) CuO/ZnO-NPs CBest

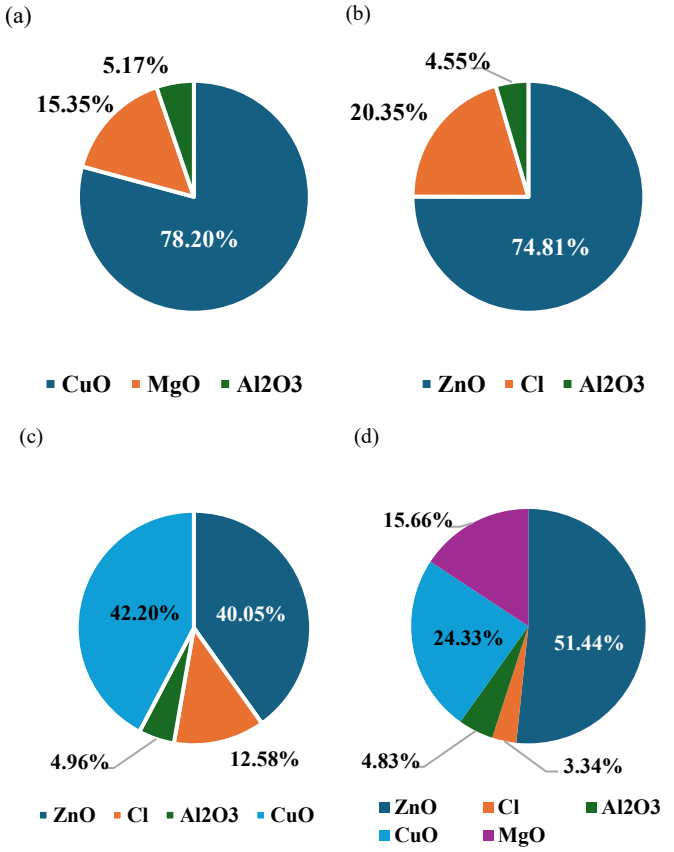

Fig. 7. Chemical composition of: (a) CuO-NPS; (b) ZnO-NPs; (c) CuO/ZnO-NPs 1:1; (d) CuO/ZnO-NPs CBest

Table 2. Comparison of CuO and ZnO moles in CuO/ZnO nanoparticles

Nanoparticle	Chemical composition	
	%Mass	Mole Comparison
CuO/ZnO (1:1)	CuO: 42.2 ZnO: 40.05	CuO: ZnO 0.53: 0.49 1.08: 1
CuO/ZnO (Cbest)	CuO: 24.3 ZnO: 51.44	CuO: ZnO 0.30: 0.63 1: 2.1

As presented in Table 2, the CuO/ZnO (1:1) nanoparticles have been shown to achieve a stoichiometric ratio that approaches the theoretical target of 1:1. This result is accompanied by a total metal oxide yield of 82.25%. Conversely, in the CuO/ZnO (Cbest) nanoparticles, a deviation was observed whereby a preference for the formation of the ZnO phase was noted over that of the CuO phase, resulting in a 2:1 ratio. This phenomenon is significantly correlated with the increased incorporation of magnesium minerals in the form of MgO into the nanoparticle matrix. The presence of MgO is assumed to act as a supporting agent or dopant that thermodynamically stabilizes the crystalline ZnO phase during the nucleation process.

3.2. Particle size analyzer (PSA)

PSA analysis was performed to determine the average size distribution of particles dispersed in a liquid medium. As

presented in Table 3, ZnO nanoparticles exhibit the smallest mean size, ranging from 2.029 to 2.086 μm. In contrast, CuO/ZnO (Cbest) nanoparticles exhibit the largest average size, reaching 4.860 μm.

Table 3. Test result of *particle size analyzer*

Nanoparticle	Median (μm)	Mean (μm)	Module (μm)	Std Dev
ZnO	2.741	2.086	5.348	0.600
	2.654	2.029	5.348	0.600
CuO	4.096	3.587	5.348	0.581
	4.143	3.543	5.348	0.550
CuO/ZnO (1:1)	4.799	4.285	5.348	0.447
	4.742	4.282	5.348	0.455
CuO/ZnO (Cbest)	6.445	4.860	10.756	0.653
	6.273	4.689	10.756	0.648

The results of the tests conducted using PSA indicated a relatively large average size (μm). This phenomenon can be attributable to the strong agglomeration of nanoparticles when dispersed in a liquid medium. In such condition, the PSA instrument measures clusters of particles as a single hydrodynamic diameter. This hypothesis was confirmed by SEM morphology, which revealed massive particle aggregation. However, further morphological analysis using ImageJ software on individual primary particles demonstrated that the actual physical diameter of the synthesized nanoparticles remained in the nanometer range.

3.3. Antibacterial activity

The copper oxide nanoparticles (CuO-NPs), zinc oxide nanoparticles (ZnO-NPs), and CuO/ZnO-NPs composites were subjected to test for antibacterial activity against Gram-positive (*Staphylococcus aureus*) and Gram-negative (*Escherichia coli*) bacteria (see Table 4). The measurement of inhibition zone was conducted in millimeters (mm) and served as the primary parameter of analysis. As illustrated in Table 4, the inhibition zones for *S. aureus* across all samples ranged from 6.90 to 10.02 mm, with the highest value achieved by CuO/ZnO-NPs (Cbest) at 10.02 mm. This finding indicates that the composition of the Cbest sample has achieved an optimal balance between the release of Cu^{2+} and Zn^{2+} ions. This synergistic interaction has been demonstrated to more effectively penetrate the thick peptidoglycan layer of Gram-positive bacteria. Bimetallic oxide nanocomposites frequently exhibit higher toxicity towards Gram-positive bacteria in comparison to their monometallic counterparts. This phenomenon can be attributed to the enhanced penetration capabilities of the former through the dense peptidoglycan network [22]. In general, the inhibition zone diameters for *S. aureus* exhibited a tendency to be smaller than those for *E. coli* (particularly for CuO-NPs). This finding is attributed to the structure of the Gram-positive cell wall, which is rich in peptidoglycan (20–80 nm) and acts as a mechanical shield against direct nanoparticle penetration.

However, a different phenomenon was observed in *E. coli* bacteria. The CuO-NPs sample exhibited the most potent activity, with an inhibition zone of 15.39 mm. The value obtained in this instance was found significantly surpassing all other tested samples. This finding indicates a high level of sensitivity exhibited by Gram-negative bacteria to copper oxide. It has been demonstrated that CuO nanoparticles exhibit an extremely high affinity for the lipopolysaccharide (LPS) groups found on the outer membrane of Gram-negative bacteria [23]. The penetration of Cu^{2+} ions triggers massive lipid peroxidation, a process which has been shown to be significantly more destructive to the thin membrane structure of *E. coli* in comparison to Gram-positive bacteria [24]. Conversely, ZnO-NPs demonstrated relatively weak activity against *E. coli* (3.01 mm). It is evident from the low inhibition value of ZnO-NPs on *E. coli* that the isolates of *E. coli* possess more efficient zinc ion efflux mechanisms compared to copper ions, thereby exhibiting higher resistance to ZnO [25]. Furthermore, the antimicrobial properties of CuO-NPs are attributable to the release of Cu^{2+} ions, reducing cell membrane permeability [26]. This process enables the ions to enter the cell, thereby inducing the generation of reactive oxygen species (ROS). These ROS subsequently lead to protein denaturation and the inhibition of the replication and transcription of genetic material.

Table 4. Antibacterial activities of CuO-NPs. ZnO-NPs. and CuO/ZnO-NPs

Materials	Bacterial Inhibition (mm)	
	Staphylococcus aureus	*Eschericia coli*
Negative control (Blank disc)	0.00	0.00
CuO-NPs	9.70	15.39
ZnO-NPs	9.08	3.01
CuO/ZnO-NPs (1:1)	6.90	8.41
CuO/ZnO-NPs (Cbest)	10.02	5.63
Positive control (Chloramphenicol)	32.26	28.60

The difference in outcomes between CuO/ZnO-NPs (1:1) and (Cbest) highlights the imperative role of optimizing material ratios, while CuO/ZnO-NPs (Cbest) demonstrated superior performance against *S. aureus*. Conversely, the 1:1 ratio yielded more optimal results against *E. coli*. The efficacy of the materials varies based on the ratio. The assertion has been made that the antibacterial activity of composites is highly dependent on the specific surface area and the formation of heterojunctions between CuO and ZnO [27]. Suboptimal ratios have been demonstrated to result in the obstruction of active sites or particle agglomeration. Furthermore, the production of Reactive Oxygen Species (ROS), such as hydroxyl radicals (OH), reaches its peak at specific crystal configurations, which explains why the CuO/ZnO-NPs (Cbest) sample exhibits varying performance across different bacterial species [28].

Table 5. *Anova one-way* test results: (a) *Staphylococcus aureus* and (b) *Escherichia coli*

	Sum of Squares	df	*Mean Square*	F	Sig.
(a)					
Between Group	17.695	3	5.898	35.977	.000
Within Group	1.312	8	.164		
Total	19.007	11			
(b)					
Between Group	255.607	3	85.202	394.060	.000
Within Group	1.730	8	.216		
Total	257.337	11			

A one-way analysis of variance (ANOVA) was conducted to evaluate the differences in antibacterial activity among the tested nanoparticles, namely CuO, ZnO, and CuO–ZnO bimetallic nanoparticles. The results of the study are presented in Table 5. ANOVA revealed a highly significant difference among the treatment groups for *Staphylococcus aureus,* with an F-value of 35.977 and a significance level of $p < 0.001$. The between-group variance (SS = 17.695) was substantially greater than the within-group variance (SS = 1.312), indicating that the observed differences in antibacterial performance were primarily attributed to the nanoparticle composition rather than experimental variability. The findings demonstrate that the antibacterial efficacy against *S. aureus* was significantly determined by the type of metal oxide nanoparticle employed.

A highly significant effect of nanoparticle composition was also observed in the case of *Escherichia coli* ($F = 394.060$, $p < 0.001$). The between-group sum of squares (255.607) was found to be considerably higher than the within-group sum of squares (1.730), thus indicating a pronounced treatment effect. The substantially elevated F-value obtained for *E. coli* in comparison to *S. aureus* indicates that the antibacterial responses of the tested materials were more distinctly differentiated against Gram-negative bacteria.

4. Conclusion

The present study demonstrated the significance role of *Moringa oleifera* leaf extract in the green synthesis of CuO, ZnO, and CuO/ZnO nanoparticles. The successful fabrication of bimetallic CuO/ZnO nanoparticles was achieved under the optimum synthesis conditions established for the individual metal oxides. Among the tested compositions, the CuO/ZnO (1:1) nanocomposite was found to exhibit the closest stoichiometric ratio to the theoretical target, with a total metal oxide yield of 82.25%, which is indicative of effective incorporation of both metal oxides within the nanocomposite structure. The antibacterial evaluation revealed that nanoparticle composition significantly determined antibacterial performance against both *Escherichia coli* and *Staphylococcus aureus* ($p < 0.05$). CuO-NPs demonstrated the most pronounced antibacterial activity against E. coli, producing an inhibition zone of 15.39 mm. In contrast, the CuO/ZnO (Cbest) nanocomposite demonstrated the highest antibacterial activity against S. aureus, with an inhibition zone of 10.02 mm. A thorough statistical analysis was conducted, which yielded substantial evidence of significant differences among the tested nanoparticle formulations. This analysis underscores the significance of nanoparticle composition in determining antibacterial efficacy.

Acknowledgements

The authors would like to express their sincere gratitude to the Ministry of Higher Education, Science, and Technology (Kemdiktisaintek) Directorate of Research and Community Service, Directorate General of Research and Development, for providing financial support for this study through the Applied Research Prototype Scheme for the fiscal years 2025–2026.

References

1. Rhamdiyah FK, Maharani DK. *Biosynthesis of ZnO nanoparticles from aqueous extract of Moringa oleifera L.: Its application as antibacterial and photocatalyst*. Indones J Chem Sci. (2022).
2. Fatoni A, Hilma H, Rasyad A, Novriyanti S. *Biosintesis ZnO nanopartikel dari ekstrak air daun jambu biji (Psidium guajava L.) dan ion Zn2+ serta interaksinya dengan kitosan sebagai antibakteri Escherichia coli*. *J Sains Farm Klin*. (2020) 151.
3. Yu W, Tang J, Gao C, Zheng X, Zhu P. *Green synthesis of copper nanoparticles from the aqueous extract of Lonicera japonica Thunb and evaluation of its catalytic property, cytotoxicity, and antimicrobial activity*. *Nanomaterials*. (2025).
4. Nguyen TT, Nguyen YN, Tran XT, Nguyen TT, Tran TV. *Green synthesis of CuO, ZnO and CuO/ZnO nanoparticles using Annona glabra leaf extract for antioxidant, antibacterial and photocatalytic activities*. *J Environ Chem Eng*. (2023) 111003.
5. Swandono HU, Fitria F, Permatasari I. *Representasi simplisia dan ekstrak etanol daun kelor (Moringa oleifera L.) terpurifikasi*. J Pharma Bhakta. (2024) 55–64.
6. Nurfadia VH, Wilapangga A, Royani S. *Green synthesis nanopartikel perak (NPAg) menggunakan ekstrak etanol 96% daun kelor (Moringa oleifera) sebagai antibakteri*. *J Pharm*. (2024) 146–156.
7. Ahmed S, Ahmad M, Swami BL, Ikram S. *Green synthesis of silver nanoparticles using plant extracts and their applications*. *J Adv Res*. (2016) 17–28.
8. Singh J, Dutta T, Kim KH, Rawat M, Samddar P, Kumar P. *Green synthesis of metals and their oxide nanoparticles: Applications for environmental remediation*. J Nanobiotechnol. (2018) 1–24.
9. Mageshwari K, Mali SS, Sathyamoorthy R, Patil PS. *Template-free synthesis of MgO nanoparticles for effective photocatalytic applications*. Powder Technol. (2013) 456–462.
10. Umar H, et al. *Plant-mediated green synthesis of ZnO nanoparticles: Progress in biomedical applications*. Bioprocess Biosyst Eng. (2022) 1–19.
11. Nasrollahzadeh M, Sajadi SM, Iravani S, Varma RS. *Green-synthesized nanocatalysts and their applications*. Chem Rev. (2019) 3738–3939.
12. Niggli P. *Die Kristallstruktur einiger Oxyde I.* Z Kristallogr Kristallgeom Kristallphys Kristallchem. (1922) 253–299.
13. Albertsson J, Abrahams SC, Kvick A. *Atomic displacement, anharmonic thermal vibration, expansivity, and pyroelectric coefficient thermal dependences in ZnO*. Acta Crystallogr B. (1989) 34–40.
14. Sangeetha G, Rajeshwari S, Venckatesh R. *Green synthesis of zinc oxide nanoparticles by Aloe barbadensis Miller leaf extract*. Mater Res Bull.

(2011) 2560–2566.
15. Diallo A, Ngom BD, Park E, Maaza M. *Green synthesis of ZnO nanoparticles by Aspalathus linearis: Structural, optical and photocatalytic properties*. J Alloys Compd. (2015) 425–430.
16. Vijayakumar S, Mahadevan S, Arulmozhi P, Sriram S, Praseetha PK. *Green synthesis of zinc oxide nanoparticles using Atalantia monophylla leaf extracts: Characterization and antimicrobial analysis*. Mater Sci Energy Technol. (2018) 22–27.
17. Sun M, Zeng Z, Zhang L. *Recent progress in bimetallic nanostructures: Synthesis, properties and applications*. Nanoscale Adv. (2019) 4064–4086.
18. Moezzi A, McDonagh AM, Cortie MB. *Zinc oxide particles: Synthesis, properties and applications*. Chem Eng J. (2012) 185–186
19. Munandar N, Aritonang HF, Bonaventura R, Wijaya DP. *Synthesis of Cu nanoparticles using Anredera cordifolia extract and their potential as antidiabetic with alpha amylase enzyme inhibition*. Commun Sci Technol. (2025) 422–430.
20. Nasrollahzadeh M, Sajjadi M, Sajadi SM, Iravani S, editors. *Green synthesis of nanoparticles*. *Elsevier*. (2021) 125–154.
21. Siddiqi KS, Rahman A, Husen A. *Properties of zinc oxide nanoparticles and their activity against microbes*. Nanoscale Res Lett. (2018) 141.
22. Gudkov SV, Shafeev GA, Glinushkin AP, et al. *A mini review of antibacterial properties of ZnO nanoparticles*. Front Phys. (2021) 641481.
23. Hatamie A, Khan A, Golabi M, Kiani A, Zobaradist P, Willander M. *Zinc oxide nanostructures for effective killing of Escherichia coli and Staphylococcus aureus*. Mater Sci Eng C. (2019) 761–772.
24. Vera-Reyes I, Lira-Saldivar RH, Mendez-Argüello B. *Nanoparticles of CuO and ZnO: Influence of oxidative stress on bacterial membrane integrity*. Nanomaterials. (2022) 652
25. Almadiy AA, Nenaah GE, Jassas MJ. *Synthesis of CuO/ZnO nanocomposites and their antibacterial activity: Influence of surface area and reactive oxygen species generation*. Mater Chem Phys. (2023)127145.
26. Slavin YN, Asnis J, Häfeli UO, Bach H. *Metal nanoparticles: Understanding the mechanisms behind antibacterial activity*. J Nanobiotechnol. (2017) 65.
27. Kulkarni S, Akolkar HN, Khedkar VM, Ramasamy R, Mahanwar KR, Darekar NR. *Biogenic-based metal nanomaterials for sustainable engineering applications*. Oakville (ON): Apple Academic Press. (2025).
28. Sharma S, Kumar K, Thakur N, Chauhan S, Chauhan MS. *Eco-friendly Ocimum tenuiflorum green route synthesis of CuO nanoparticles: Characterizations on photocatalytic and antibacterial activities*. J Environ Chem Eng. (2021) 105395.